

Mapping Molecular Binding by Means of Conformational Dynamics Measurements

Noelle M. do Nascimento¹, Augusto Juste-Dolz¹, Paulo R. Bueno², Isidro Monzó³, Roberto Tejero³, José L. Lopez-Paz¹, Angel Maquieira¹, Sergi Morais^{1*}, David Gimenez-Romero^{3*}

¹ Instituto Interuniversitario de Investigación de Reconocimiento Molecular y Desarrollo Tecnológico, Departamento de Química, Universitat Politècnica de València, Camino de Vera, s/n Valencia, 46022, Spain.

²Instituto de Química, Univ. Estadual Paulista (UNESP), Departamento de Físico-Química, Nanobionics Research Group (www.nanobionics.pro.br), Araraquara, São Paulo, Brazil.

³Departamento de Química-Física, Universitat de València, C/ Dr. Moliner 50, 46100 Burjassot, Spain.

**Corresponding author.*

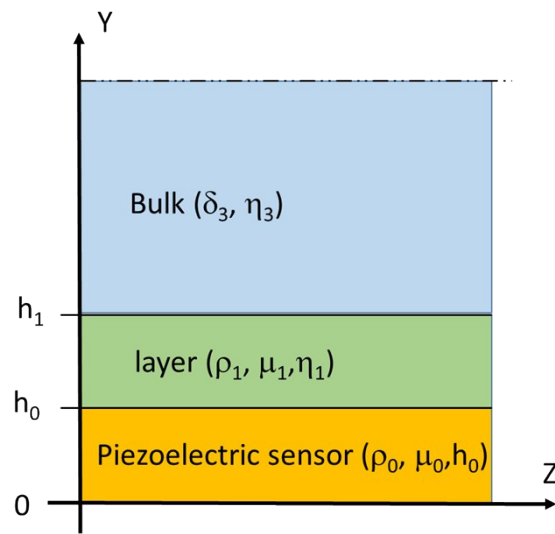
E-mail address: David.Gimenez-Romero@uv.es (D. Giménez-Romero)

smorais@gim.upv.es (S. Morais).

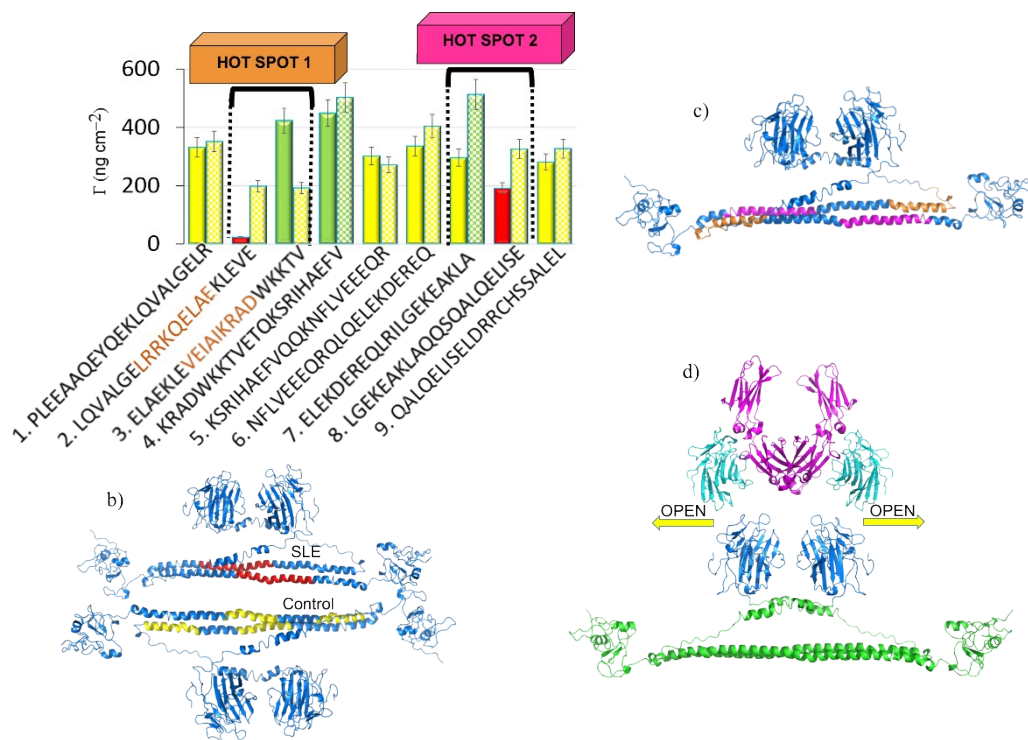
INDEX

I. SUPPORTING FIGURES	3
II. SUPPORTING TABLES	6
III. SUPPORTING NOTES	9
IV. REFERENCES	15

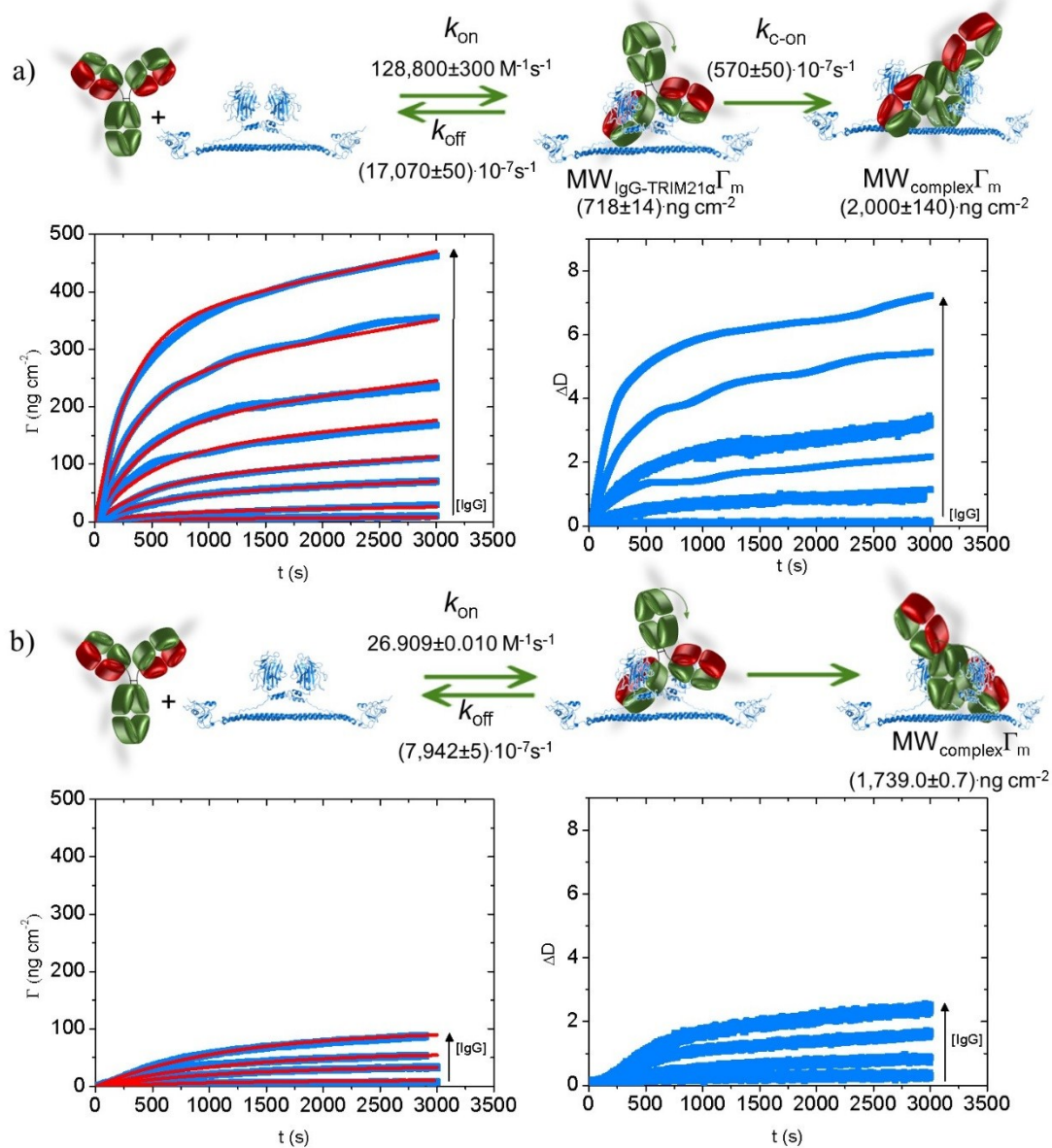
I. SUPPORTING FIGURES



S1 Figure. Geometry of a piezoelectric crystal covered by a viscoelastic film. ρ is density, h thickness, μ is the shear elasticity modulus and η is the elastic shear viscosity.



S2 Figure. a) Linear epitope mapping for the SLE patients (solid-fill) and healthy subjects (pattern-fill) -see S1 Table-. Red, yellow and green bars show weakly ($<166 \text{ ng cm}^{-2}$), moderate ($166 \text{ ng cm}^{-2} \leq \text{Intensity} \leq 330 \text{ ng cm}^{-2}$) and strong ($> 330 \text{ ng cm}^{-2}$) interactions between the protein and autoantibodies, respectively. Hot spots comprise the polypeptides 2, 3, 7 and 8, which show the sequences that are predicted to have a different affinity for the sera of the SLE patients or healthy subjects. b) The different epitopes recognized by the autoantibodies of the SLE patients (red) and healthy subjects (yellow). c) The location of hot spot #1 (pink) and hot spot #2 (orange) in the TRIM21 α structure. d) The scheme of the homodimer-IgG biorecognition. The PRY-SPRY domains open to interact with the Fc fragment (violet in colour) of the antibody.



S3 Figure. The real-time relaxation curves (surface concentration, Γ , and dissipation shift, ΔD , according to time) of the IgG-TRIM21 α interaction for different antibody concentrations. The values of the association (k_{on}) and dissociation (k_{off}) rate constants, and the molecular weight parameter for the maximum surface concentration ($MW_{IgG-TRIM21\alpha} \Gamma_m$ for the reaction intermediates and $MW_{complex} \Gamma_m$ for the final antigenic complexes) were obtained from the purified IgGs of a) the SLE patients and b) healthy subjects. Red lines are the fittings from the kinetic parameters shown in the reaction schemes. Only one point out of ten measured points was taken for all the plots.

II. SUPPORTING TABLES

S1 Table. The solid-phase synthetic polypeptides sequences used in the screening of the coiled-coil region of the TRIM21 α protein (from amino acid 127 to 243). Each polypeptide sequence contains 21 amino acids, and overlaps with the last nine amino acids of former one, and with the first nine amino acids of the following one. Only one track of three amino acids in the middle of the sequence does not overlap.

N°	Sequences	a.a.
1	PLEEAAQEYQEKLQVALGELR-NH2	127-147
2	LQVALGELRRKQELA EKLEVE-NH2	139-159
3	ELAEKLEVEIAIKRADWKKTV-NH2	151-171
4	KRADWKKTVETQKSRIHAEFV-NH2	163-183
5	KSRIHAEFVQQKNFLVEEEQR-NH2	175-195
6	NFLVEEEQRQLQELEKDEREQ-NH2	187-207
7	ELEKDEREQLRILGEKEAKLA-NH2	199-219
8	LGEKEAKLAQQSQALQELISE-NH2	211-231
9	QALQELISELDRRCHSSALEL-NH2	223-243

S2 Table. The control parameters of the fitting of the QCM–D data obtained from the IgG-TRIM21 α biorecognition event. The kinetic parameters were fitted with 80,000 data points. Fitting was done by considering data points with three coordinates: time, the surface concentration of the antigenic complex and the biomarker concentration in the bulk. The relative deviations of the simulation kinetic parameters were lower than 3% in all cases.

	χ^2	Degrees of freedom	Residual sum of squares $\text{ng}^2 \text{cm}^{-4}$	Akaike information criterion	Second order Akaike information criterion
SLE patients	34,801	63,800	159,265	23,899	23,899
Healthy subjects	11,222	41,339	170,569	58,598	58,598

S3 Table. The parameters calculated from the fittings of the QCM-D data obtained for the IgG-TRIM21 α biorecognition event.

IgG	k_{on} M⁻¹ s⁻¹	$10^7 k_{off}$ s⁻¹	$10^7 k_{c-on}$ s⁻¹	N	$MW_{IgG-TRIM21}\Gamma_m$ ng cm⁻²	$MW_{complex}\Gamma_m$ ng cm⁻²
SLE	128,800±300	17,070±50	570±50	1.328±0.006	718±14	2,000±140
Control	26.909±0.010	7,942±5	--	1.35±0	--	1,739.0±0.7

III. SUPPORTING NOTES

S1 NOTE. THEORETICAL $-\frac{d\Delta f}{d\Delta D}$ FUNCTION

As S1 Figure shows, we considered the case of a viscoelastic layer that covered the surface of a piezo-electric plate and oscillated in a pure shear mode in a bulk liquid. Thus the acoustic response of the QCM-D when a piezoelectric sensor (density ρ_0 , thickness h_0 and shear elasticity modulus μ_0) was covered by a thin viscoelastic layer (density ρ_1 , thickness h_1 , elastic shear viscosity η_1 and shear elasticity modulus μ_1) immersed in a Newtonian bulk liquid (elastic shear viscosity η_3 and viscous penetration depth and δ_3) corresponds to:¹

$$\Delta f \approx -\frac{1}{2\pi\rho_0 h_0} \left[\frac{\eta_3}{\delta_3} + h_1 \rho_1 w - 2h_1 \left(\frac{\eta_3}{\delta_3} \right)^2 \frac{\eta_1 w^2}{\mu_1^2 + w^2 \eta_1^2} \right] \quad \text{Eq. (1)}$$

$$\Delta D \approx \frac{1}{2\pi f \rho_0 h_0} \left[\frac{\eta_3}{\delta_3} + 2h_1 \left(\frac{\eta_3}{\delta_3} \right)^2 \frac{\mu_1 w}{\mu_1^2 + w^2 \eta_1^2} \right] \quad \text{Eq. (2)}$$

where w is the angular resonant frequency ($2\pi f$).

According to Eqs. (1) and (2), the contribution of a ultrathin film was minor in comparison to the bulk liquid acoustic response. Therefore:

$$\Delta f \approx -\frac{1}{2\pi\rho_0 h_0} \frac{\eta_3}{\delta_3} \quad \text{Eq. (3)}$$

$$\Delta D \approx \frac{1}{2\pi f \rho_0 h_0} \frac{\eta_3}{\delta_3} \quad \text{Eq. (4)}$$

Evidently, both parameters depended on the viscoelastic properties of the bulk liquid under these experimental conditions. However, a thin layer with a finite thickness would demonstrate a different acoustic response depending on the ratio between the viscosity and the elasticity of the film. To provide a clearer picture, let's start with only one purely elastic film ($\eta_1 \rightarrow 0$):

$$\Delta f \approx -\frac{1}{2\pi\rho_0 h_0} \left[\frac{\eta_3}{\delta_3} + h_1 \rho_1 w \right] \quad \text{Eq. (5)}$$

$$\Delta D \approx \frac{1}{2\pi f \rho_0 h_0} \left[\frac{\eta_3}{\delta_3} + 2h_1 \left(\frac{\eta_3}{\delta_3} \right)^2 \frac{w}{\mu_1} \right] = \frac{1}{\rho_0 h_0} \left[\frac{\eta_3}{\delta_3} \frac{1}{2\pi f} + 2h_1 \left(\frac{\eta_3}{\delta_3} \right)^2 \frac{1}{\mu_1} \right] \quad \text{Eq. (6)}$$

Next both expressions are derived according to the monitoring time:

$$\frac{d\Delta f}{dt} \approx -\frac{1}{2\pi\rho_0 h_0} \frac{d(h_1 \rho_1 w)}{dt} \quad \text{Eq. (7)}$$

$$\frac{d\Delta D}{dt} \approx \frac{1}{2\pi f \rho_0 h_0} 2 \left(\frac{\eta_3}{\delta_3} \right)^2 \frac{d}{dt} \left(\frac{h_1 w}{\mu_1} \right) \quad \text{Eq. (8)}$$

Therefore, the ratio between both expressions corresponds to:

$$\frac{d\Delta f}{d\Delta D} = \frac{\frac{d\Delta f}{dt}}{\frac{d\Delta D}{dt}} \approx \frac{-\frac{1}{2\pi\rho_0 h_0} \frac{d(h_1 \rho_1 w)}{dt}}{\frac{1}{2\pi f \rho_0 h_0} 2 \left(\frac{\eta_3}{\delta_3} \right)^2 \frac{d}{dt} \left(\frac{h_1 w}{\mu_1} \right)} = \frac{f}{2} \left(\frac{\delta_3}{\eta_3} \right)^2 \frac{d(h_1 \rho_1 w)}{dt} \frac{d}{dt} \left(\frac{h_1 w}{\mu_1} \right) = \quad \text{Eq. (9)}$$

$$= \frac{-f}{2} \left(\frac{\delta_3}{\eta_3} \right)^2 \frac{w \frac{d(h_1 \rho_1)}{dt} + h_1 \rho_1 \frac{dw}{dt}}{w \frac{d}{dt} \left(\frac{h_1}{\mu_1} \right) + \frac{h_1}{\mu_1} \frac{dw}{dt}} \approx \frac{-f}{2} \left(\frac{\delta_3}{\eta_3} \right)^2 \mu_1 \rho_1$$

$$-\frac{d\Delta f}{d\Delta D} \approx \frac{f}{2} \left(\frac{\delta_3}{\eta_3} \right)^2 \mu_1 \rho_1 \quad \text{Eq. (10)}$$

The application of Eq. (10) requires films with a thickness of not more than a few nanometers in order to yield a fair agreement with the full equation. Still it holds quite generally that the shift in bandwidth is affected mostly by the elastic compliance of the film, rather than by its viscous compliance. So Eq. (10) is a measurement of the instantaneous stiffness of the adlayer. Hence if only one interfacial process is monitored, this novel function will allow the identification of reaction intermediates, as well as the formed reacting products. These intermediates and products have different structures from the initial adlayer. Therefore, its formation necessarily involves a structural transition, which will be monitored by this function. Accordingly, it is possible to state that this novel plot highlights mechanistic processes. Its trace can be used as a fingerprint for the studied interaction, as used in the Δf - ΔD plots.

S2 NOTE. DETERMINATION OF THE THICKNESS PER MOLECULE

As demonstrated above, Eq. (10) allowed the reaction intermediates to be easily identified. However, nothing was stated about the conformation acquired by the different ligands during the interfacial process. To this end, we could study these processes by DPI as this technique monitors adlayer dry thickness h_1 in real-time, which is related to the conformational dynamics of the studied interface processes, Eq. (11):²

$$\Delta h = \frac{1}{N_T} \sum \Delta m_i \left(\frac{\Delta h}{\text{molecule}} \right)_i \quad \text{Eq. (11)}$$

The biophysical characterization of the protein–ligand relations by DPI is based on immobilizing one component on a biosensor surface, whereas a captured ligand is in the bulk. Thus any changes in adlayer thickness are caused by the binding of only one ligand. We consider this special case, and from Eq. (11) we therefore obtained:

$$\left(\frac{\Delta h}{\text{molecule}} \right)_1 = \frac{N_T}{\Delta m_1} h_1 \quad \text{Eq. (12)}$$

where N_T , h_1 and Δm_1 are the parameters measured by DPI.

The thickness per molecule of the antigenic complexes, $\left(\frac{\Delta h}{\text{molecule}} \right)_1$, can be so monitored by DPI. Thus and if these values are compared with the theoretical dimensions of the ligand, protein conformations can be monitored in real-time.

S3 NOTE. LINEAR EPITOPE MAPPING

The serological epitope profile of the anti-TRIM21+ patients showed that the immunodominant epitope can be located on the coiled-coil domain.³⁻⁵ Accordingly, the amino acid sequence of the coiled-coil domain (see S1 Table) was mapped for the IgG-binding linear epitopes. To this end, nine overlapping solid-phase synthetic polypeptides were tested by monitoring the piezoelectric signal of the QCM-D sensor and sampling the purified IgGs from the SLE patients and healthy subjects. As presented in S2a Figure, the SLE IgG reacted

strongly with polypeptides 3 and 4, weakly with polypeptides 2 and 8, and the moderately with the others. It should be noted that differences in the intensity of the reaction could reflect the affinity of the reactants, the relative amount of the autoantibody present in the bulk, or a combination of both parameters. The reactive peptides (151-171 and 163-183 a.a.) partially overlapped the adjacent reactive sequences, and together could represent an unknown immunodominant linear epitope on the TRIM21 α in the SLE patients. Note that the $-\frac{d\Delta f}{d\Delta D}$ value for this immunodominant polypeptide corresponded to 22 Hz⁻¹, which is similar to that measured using TRIM21 α as a probe: 20 Hz⁻¹. Hence, it is possible to state that the conformational changes monitored in the TRIM21 α :IgG interaction in the sera of the SLE patients corresponded mainly to the changes in autoantibody conformation, and is probably not due to any conformational changes in the probe (TRIM21 α or polypeptide). This confirms conformational changes, which may require the protein structure to promote the autoantibody bipolar bridging mechanism.

Similarly, the solution of the IgGs from the healthy subjects was tested for autoantibody-binding to linear epitopes by probing the same nine overlapping solid-phase synthetic TRIM21 α polypeptides. As presented in S2a Figure, the control IgG reacted strongly with the polypeptides 4 and 7, and moderately with the others. These results confirm that circulating autoantibodies were present in the healthy subjects and targeted the TRIM21 α protein, as previously reported.⁶ Furthermore, the two detected discontinuous reactive sequences (163-183 and 199-219 a.a.) could represent two different linear immunodominant epitopes, or either a conformational epitope (see S2b Figure).

In order to compare the recognition of the autoantibody-binding peptides of the SLE and control autoantibodies, S2b Figure shows the alignment of the sequences and highlights the corresponding autoantibody-binding regions. To clarify the discussion, two hot spots were

highlighted (see S2a and S2c Figure), which corresponded to the antigenic regions that exhibited a significantly different affinity between the SLE patients and the healthy subjects. These regions identified the different epitopes between the two groups, which could match with the location of the disease-associated polymorphisms in the TRIM21 gene (11p15.4 OMIM 109092).

The ProPred web-based algorithm was used to predict the motifs within the sequence of TRIM21 α , which have a high affinity for a comprehensive panel of HLA-DR molecules, including all those expressed by the SLE patients and healthy subjects.⁷ The predicted results revealed that sequences LRRKQELAE (a.a. 146-154, expressed as the HLA-DRB1*0806 and HLA-DRB1*0816 alleles) and VEIAIKRAD (a.a. 158-166, HLA-DRB1*1304 allele) had a higher affinity for any of the MHC class II molecules under study. Interestingly, both sequences were located in hot spot region #1, which corroborates the specific epitopes located *in vitro* on the TRIM21 α protein.

S4 NOTE. KINETICS

According to the experimental data, it remains unclear whether the two elementary steps corresponded to consecutive or parallel processes. In order to explore the molecular recognition process, we used the Akaike information criterion to select the molecular mechanism of the protein-protein interaction (see S2 Table). The evolution of the piezoelectric signal according to the reaction time was simultaneously modelled at different autoantibody concentrations for the SLE patients and healthy subjects. To this end, a two-step consecutive reaction model for the autoantibodies of the SLE patients was selected (S3a Figure), where autoantibody-TRIM21 α simultaneously bound via their Fab (higher affinity) and Fc (lower affinity) regions in a bipolar bridging mechanism.⁸ The selected model, used when the antibodies came from healthy subjects, presented subtle differences (S3b Figure).

While the reaction mechanism proposed by the QCM-D modelling for the autoantibodies of the SLE patients considered a bivalent recognition process, a single reaction step was involved for the healthy subjects. The conformational changes that involved the intermediate state in the healthy subjects were much less marked than in the SLE patients, as Figure 1b shows in the manuscript. Although both autoantibodies have different reaction pathways, the presence of two reaction steps is demonstrated above (see Figure 1d).

S3 Figure shows the good agreement observed between the fitted curves and the real curves, which confirms that the proposed binding schemes predict autoantibody-TRIM21 α system behaviour correctly for a wide range of autoantibody concentrations (see S3 Table). The experiments ran with increasing concentrations of the autoantibodies of the healthy subjects fitted a bimolecular association with a rate constant (k_{on}) and a dissociation rate constant (k_{off}) of 26.909 M⁻¹ s⁻¹ and 7.942·10⁻⁴ s⁻¹, respectively, and yielded a kinetic dissociation constant (K_d) of 29 μ M. However, for the SLE patients autoantibodies, the first association constant corresponded to 128,800 M⁻¹ s⁻¹ whereas the dissociation constant was 17.070·10⁻⁴ s⁻¹ (K_d = 13 nM), which resulted in a similar k_{on} and K_d to those reported by Keeble *et al.* during the TRIM21-mouse antibody association.⁹ By considering these data, the affinity of the anti-TRIM21 α autoantibodies for the TRIM21 α protein was much higher than that of the control autoantibodies; i.e., they should be different antibodies. To confirm this, the linear epitope mapping for both the SLE patients and healthy subjects is presente in S4 Note that the anti-TRIM21 α autoantibodies of both the SLE patients and healthy subjects had different epitopes (see S2 Figure). This often proves that they are not the same antibody and, therefore, their reaction pathways may differ, as the $-\frac{d\Delta f}{d\Delta D}$ plot shows clearly in Figure 1.

IV. REFERENCES

1. Voinova, M.V.; Rodahl, M.; Jonson, M.; Kasemo, B. Viscoelastic acoustic response of layered polymer films at fluid-solid interfaces: Continuum mechanics approach. *Physica Scripta*, 1999, **59**, 391-396.
2. Gimenez-Romero, D.; Gonzalez-Martinez, M.A.; Bañuls, M.J.; Monzo, I.; Puchades, R.; Maquieira, A. Modeling of the Role of Conformational Dynamics in Kinetics of the Antigen–Antibody Interaction in Heterogeneous Phase. *J. Phys. Chem. B* 2012, **116**, 5679-5688.
3. Routsias, J.; Tzioufas, A. G. B-cell epitopes of the intracellular autoantigens Ro/SSA and La/SSB: tools to study the regulation of the autoimmune response. *J. Autoimmun.* 2010, **35**, 256-264.
4. Fritsch, C.; Hoebeke, J.; Dali, H.; Ricchiuti, V.; Isenberg, D.A.; Meyer, O.; Muller, S. 52-kDa Ro/SSA epitopes preferentially recognized by antibodies from mothers of children with neonatal lupus and congenital heart block. *Arthritis Res. Ther.* 2006, **8**, 1-11.
5. Sung-Rok, H.; Suk-Jung, C.; Jeong, H.D.; Hong, S. Development of QCM biosensor to detect a marine derived pathogenic bacteria *Edwardsiella tarda* using a novel immobilisation method. *Biosens. Bioelectron.* 2009, **24**, 1635-1640.
6. Do Nascimento, N.M.; Juste-Dolz, A.; Grau-García, E.; Roman-Ivorra, J.A.; Puchades, R.; Maquieira, A.; Morais, S.; Gimenez-Romero, D. Label-free piezoelectric biosensor for prognosis and diagnosis of Systemic Lupus Erythematosus. *Biosens. Bioelectron.* 2017, **15**, 166-173.
7. Singh, H.; Raghava, G.P.S. ProPred: prediction of HLA-Dr Binding site. *Bioinformatics* 2001, **17**, 1236-37.
8. James, L.C.; Keeble, A.H.; Khan, Z.; Rhodes, D.A.; Trowsdale, J. Structural basis for PRYSPRY-mediated tripartite motif (TRIM) protein function. *Proc. Nat. Acad. Sci.* 2007, **104**, 6200-6205

9. Keeble, A.H.; Khan, Z.; Forster, A.; James, L.C. TRIM21 is an IgG receptor that is structurally, thermodynamically, and kinetically conserved. *Proc. Nat. Acad. Sci. USA* 2008, **105**, 6045-6050.